Astrometric Error in Observations of the Galactic Center and Experimental Implications

Cambier, H. J.[1]

hcambier@uoregon.edu

ABSTRACT

Analysis on the scale and behavior of astrometric uncertainty for Keck Telescope adaptive optics imagery of the Galactic Center (at 2.2μm) indicates a median floor error less than 0.2 milliarcseconds (mas) for all stars with apparent K' magnitude ($m_{K'}$) less than 14, or less than 0.25 and 0.40 mas for magnitude bins 14-15, and 15-16, respectively. Analysis also shows that these floors can be approached at a rate inversely proportional to the square root of frames taken. For $m_{K'} < 14$ and viewing regions less than an arcsecond (arcsec.) across, or $14 < m_{K'} < 15$ and 1/5 an arcsec., separation uncertainties are primarily propogated uncertainty of individual positions with no additional distortion. These individual and relative uncertainties define a level at which orbital shifts due to relativistic effects and extended mass distributions should become just noticeable, if not measureable.

Dispersion effects were also investigated, as they act to multiply random error caused by atmopsheric turbulence.

Subject headings: Galaxy: center — infrared: stars — non-Keplerian orbits — astrometry — techniques: high angular resolution

1. Introduction

For many years, black holes remained purely hypothetical since finding empirical evidence for objects whose gravities capture light is understandably difficult. However, this immense gravity, as well as the emissions from excited accreting matter should betray them, and these properties guided the search for black holes towards the centers of galaxies like

[1]43940 21st St. West, Lancaster CA 93536. Research funding provided by the National Science Foundation as part of the Research Exchange for Undergraduates program

our own.

The immense gravity mentioned is most measureable in the orbits of the S0 group, the closest observable stars to the black hole, most of whose $m_{K'}$ values range from 14 to 16 (Ghez et al. 2005). Measuring their positions has placed constraints on the extent of a massive gravitational source and it's separation from the radio source Sgr A*, and these constraints have been refined from 100 milliarcseconds (mas) (Ghez et al. 1998) to 50 mas (Ghez et al. 2000), and most recently, to within 2 mas (Ghez et al. 2005) by the Keck 10m telescope using a laser-guide-star adaptive-optics (LGS AO) system. Two mas is about four times the expected periastron positional shift of the star SO-2 (see §3) so having uncertainties an order of magnitude smaller could mean revealing the non-closed nature of orbits, while an order or two further would make for reliable measurements.

To this end, it is important not only to quantify the final empirical uncertainties, but to analyze them so that the instrument, or future ones, can achieve the highest precision possible; precisions that might allow the measurement of said orbital shifts.

Section 2 describes the data processing procedure. The anticipated orbital shifts are described in §3, §4 covers the error analyses performed, and §5 is the conclusion.

2. Procedure

The data sets under scrutiny both consist of 10 arcsec. x 10 arcsec. science frames taken through the K' ($\lambda_0 = 2.124\mu m$) wideband filter ($\Delta\lambda = 0.35\mu m$), on the NIRC2 camera at Keck with the LGS AO system employed. 138 images from 24 June 2006 formed one set, and 120 images from 02 May 2006 formed the other. In each case, the telescope took three shots between dithering.

The images were cleaned and reduced from multiple into single images ("maps") using the program, pyraf (Pyraf homepage). In order to later examine the effect of frame count on uncertainty, the frames were reduced in groups containing all, a third, a sixth, or a twelfth of the entire count. For the first division of the total frames into thirds, the first, second, and third shot in each dither were used to build the first, second, and third maps in order to better isolate factors that changed throughout the night or with telescope position. The subsequent divisions, though, were made along the chronological order of frames.

To quantify error three "submaps"were also made for every map, each using only a third of the frames (divided chronologically), and the variance of stellar positions between submaps defined the uncertainty. This raised some concern since, if the error relates to the frame count in the suspected statistical manner, dividing the frames again increases the uncertainty. However, because the submaps consistently use a third of the frames, $1/\sqrt{N}$ proportional errors would follow the same trend, only scaled up by a consistent overestima-

tion.

The program, Starfinder (Diolaiti et al. 2000), translated the main maps into lists with the stars and their data, and it determined an average point-spread function (PSF) using eight bright stars (IRS16C, IRS16NW, IRS16NE, IRS33E, IRS33W, S1-21, IRS29N, IRS16SW). An image source was declared a star for correlations of 0.8 or better with the PSF, while only a correlation of 0.6 was demanded for submaps. An alignment routine was run, which performed only translation transformations guided by a few stars.

3. Orbital Shifts

Orbits are already fit to the stars around Sgr A* (Ghez et al. 2003), so orbital shifting is not a new observable, but fine detail in a current one. Orbits and orbital shifts provide information on the distribution of enclosed by the orbits. There are two types of shifts: prograde, and retrograde.

General Relativity predicts for the periastron of a body's orbit around a larger point-like mass to rotate in the same angular direction (and orbital plane) that the body travels. If the enclosed mass is point-like (M_{pt}) then the prograde angular shift, $\Delta\phi$, and the separation between periastron, Δs, are given by (Rubilar & Eckart 2001):

$$\Delta\phi = \frac{6\pi G M_{pt}}{c^2 a(1-e^2)},\ and$$
$$\Delta s = \frac{6\pi G M_{pt}}{c^2(1-e)},$$

where G is the gravitational constant, a the semi-major axis, and e the eccentricity. For the star, S0-2, which has a comparitively small period of 15 years and reported eccentricity of 0.87 (Ghez et al. 2005), and the minimum constrained mass for the black hole ($2.6\times10^6 M_\odot$) (Ghez et al. 1998), this translates to an angular separation of 0.47 milliarcseconds between subsequent periastron.

A retrograde shift is one in which the star's orbital axes rotate opposite the angular direction (again, in the orbital plane) that the star travels. A primarily radially-dependent, ("non-pathological"), extended mass distribution would cause retrograde shifting. Studies (Jiang & Lin 1985; Rubilar & Eckart 2001) on shifts resulting from a purely uniform density distribution, or a Plummer-type mass distribution around the black hole mass;

$$\rho(r) = const.\ for\ r < some\ R,\ and\ 0\ elsewhere,$$

$$\rho(r) = 1/[1+(r/r_c)^2]^{\alpha/2} \quad (r_c\ and\ \alpha\ are\ parameters),$$

reveal that it is not difficult for the net shift to be in the retrograde direction. A star passing through the uniform density distribution would an experience a shift on the order of degrees. For a star traveling through the Plummer-type distribution with 99 to 90 percent of the total mass in the black hole itself, α greater than 4, and r_c less than 150 mas, the retrograde shift would equal or dominate the prograde one.

For fitting a mass distribution to the orbits, one will need at least as many stellar orbits as there are paramters (the Plummer-distribution comes with the caveat that stars of equivalent oribtal energy or angular momentum do not provide unique information (Rubilar & Eckart 2001)). If shifts require a full period for accurate measurement, then solving four unknowns (or less) would already take 40 years based on the reported periods for members of the S0 cluster (Ghez et al. 2005). Another parameter makes it 200 years.

4. Error Analysis

4.1. Error and Magnitude

Intuitively, dimmer stars, which stand out less against background noise, should have larger astrometric uncertainties. The magnitude-dependent component of the positional error is the ratio of the full-width-half-maximum (FHWM) to the signal-to-noise ratio (SNR), and based on the SNR's definition given in (Hardy 1998, p. 42) this error obeys:

$$\sigma_{mag} = \frac{FWHM}{D} \sqrt{\frac{1}{t\eta}(x + N_B a^2 x^2)} \tag{1}$$

$$with\ x = F_o * 10^{M_{K'}/2.5}$$

Here, N_B is the background (sky) irradiance, a^2 is the area of the measuring element, D is the telescope aperture diameter, η is detector effeciency, and t is the integration time. However, a curve of this form plus a constant to represent other, magnitude-independent error did not apply well to the graphs as reduced χ^2 values were on the order of a hundred.

The graph displays a dramatic floor centered roughly at $m_{K'}$=15 and a few, lower-magnitude, but high-uncertainty stars isolated from the others on the graph. Taking median instead of mean uncertainties reduces the effect of the large (rare for low-magnitude) errors, by essentially neglecting them, so some justification is appropriate.

The suspected cause is confusion and PSF contamination with the unresolved background population. Which stars are afflicted with these errors is quite consistent within a night, bolstering the case that this is not caused by the atmosphere or instrumentation. The analysis done was able to detect these large uncertainties, so the remaining analyses are performed under the assumption that this detection happens most of the time. Always

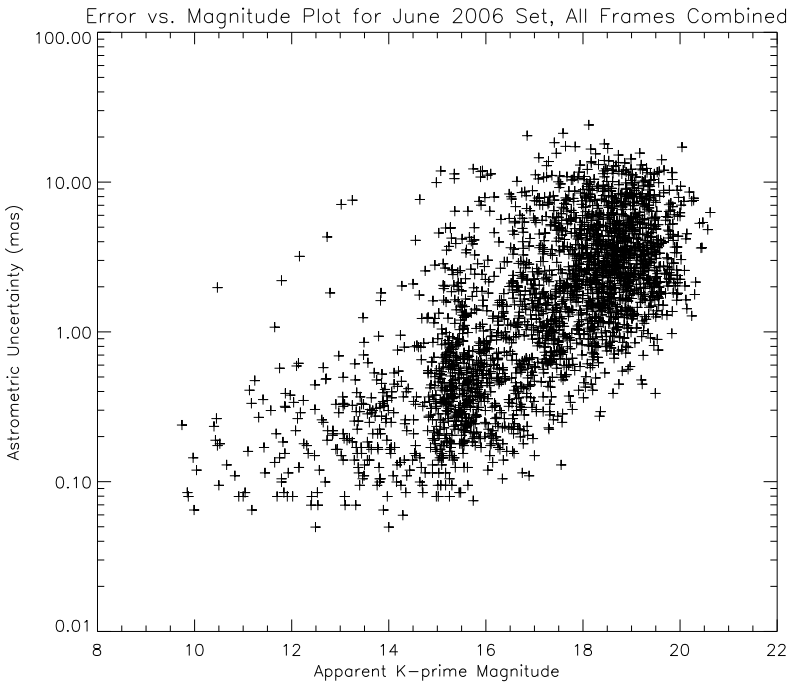

Fig. 1.— 4.1

catching these large uncertainties is still not much consolation, but if the confusion hypothesis is correct, then because the stars of interest move, they should not suffer the effect all the time.

4.2. Error and Frame Count

Using the median uncertainties, and having broken up the data as outlined in §2, the median error is plotted (figures 2 and 3) and tabluated (table 1) for stars with $m_{K'} \leq 14$, and for bins 1 magnitude wide with $m_{K'}$ values of 13 through 16. The data exhibits a $1/\sqrt{frames}$ proportionality. Linear regression to $A + Bx$ with $1/\sqrt{frames}$ as the variable produces the equations presented in table 1. Fits in which no base error was assumed ($A = 0$) had χ^2 values ten to a hundred times larger

4.3. Separation Error

Low local, or low individual astrometric uncertainties are useless if relative positions are needed over large portions of the field and are highly uncertain. Also, we expect a kind

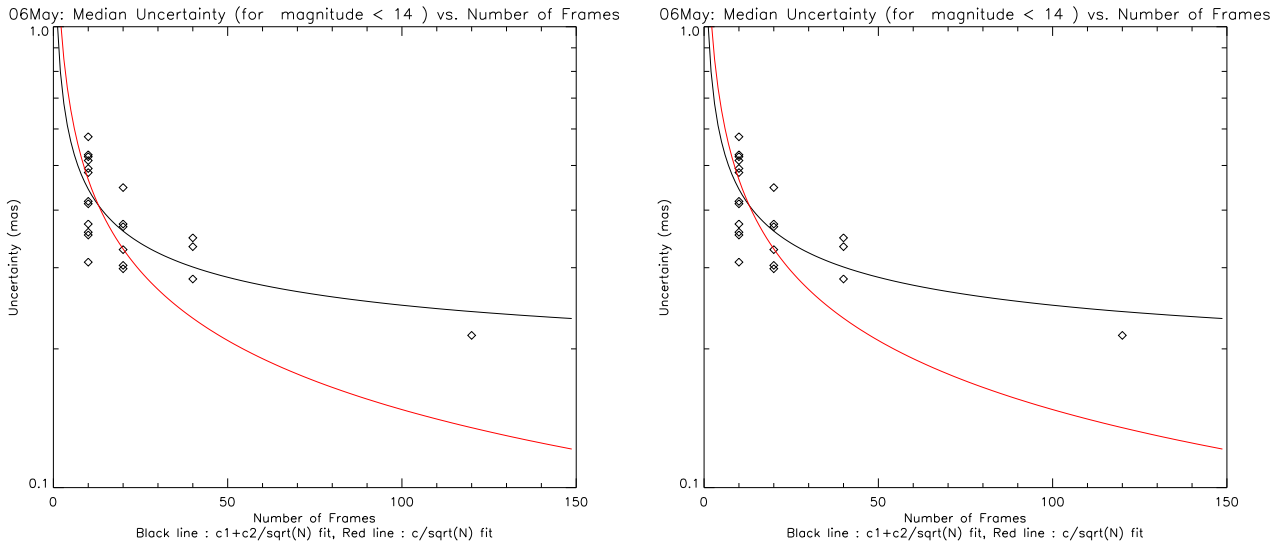

Fig. 2.— The upper (black) set of curves are the fits made with a floor error, and the red (lower) curves represent fits made assuming no floor error.

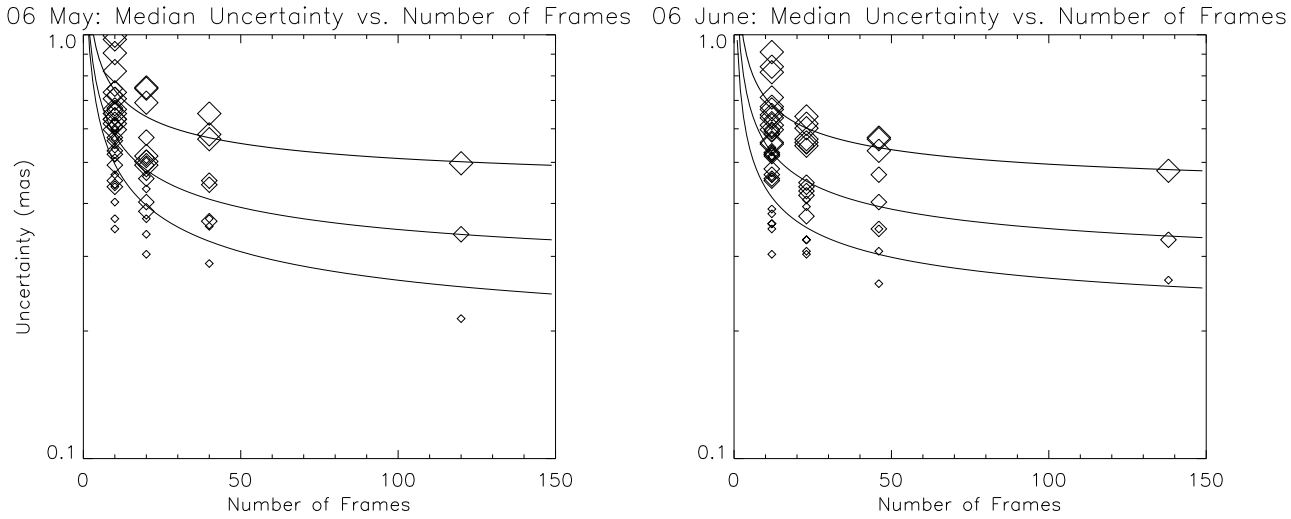

Fig. 3.— Plots for magnitude bins 13-14, 14-15, and 15-16. Higher, thicker curves and larger diamonds correspond respectively to the fits and data points for higher magnitude bins.

of relative distortion that scales up with separation due to residual wavefront error (curvature). To examine these issues, the separations were computed for every pair of stars in the six 'sixths' maps, as well as the propogated uncerainties which would feature later in the analysis.

Analyzing the effect of angular separation from the laser guide star (roughly at the image centers) and the tip/tilt guide star would be especially useful. However, the generation of the PSF from eight bright stars spread across the field complicates this since the expected distortions become partially "absorbed "by the PSFs.

Plotted in figure 4 and figure 5 4.3 is the root-mean-square (RMS) of separations normalized by the propogated uncertainties, (P_i),

$$\sigma_N = \sqrt{\frac{1}{N-1}\sum_{i=1}^{N}\left(\frac{S_i - \bar{S}}{P_i}\right)^2}. \tag{2}$$

This quantity is essentially the reduced χ for some hypothetical function that is determining the distances between stars. Where the expression is around unity or less is where this "function" is doing a good job by not distributing separation values further from the average than their propogated uncertainties would. For stars with $m_{K'} < 14$, no pair's σ_N exceeds unity until they are three-fourths to one arcsecond apart; the size of the region of interest. For stars with $14 < m_{K'} < 16$, this separation drops to about one-fifth of an arcsecond.

4.4. Dispersion Effects

Because stars deposit more photons at wavelengths as determined by their flux curves, a different portion of photons from each star will arrive at a particular angle due to refraction. This produces a shift in the North component of the star's apparent location, and since the filter has nonzero bandwidth, it always captures this effect. Analytically, dispersion should be an effect on par In the context of this section "separation" is understood to refer to its North-component.

Some of the separations between stars IR1, 16C, 16CC, 16SW, and 16NE were compared in a sample of single images from the May data. All but IR1 are $m_{K'} < 11$ sources in the Galactic center, reddened by extinction, while IR 1 is a bluer, foreground star with $m_{K'} \approx 14$. Besides their relatively low magnitudes, another criterion was low separation of each pairing (included in table 2) in order to isolate the effect already seen in the last section. The May data was chosen because it sampled a larger range of airmasses.

Taking the flux and filter weighted sum, or integral, of the photons' wavelengths gives the source's effective wavelength at which is seen and refracted. Here, the filter tranmission,

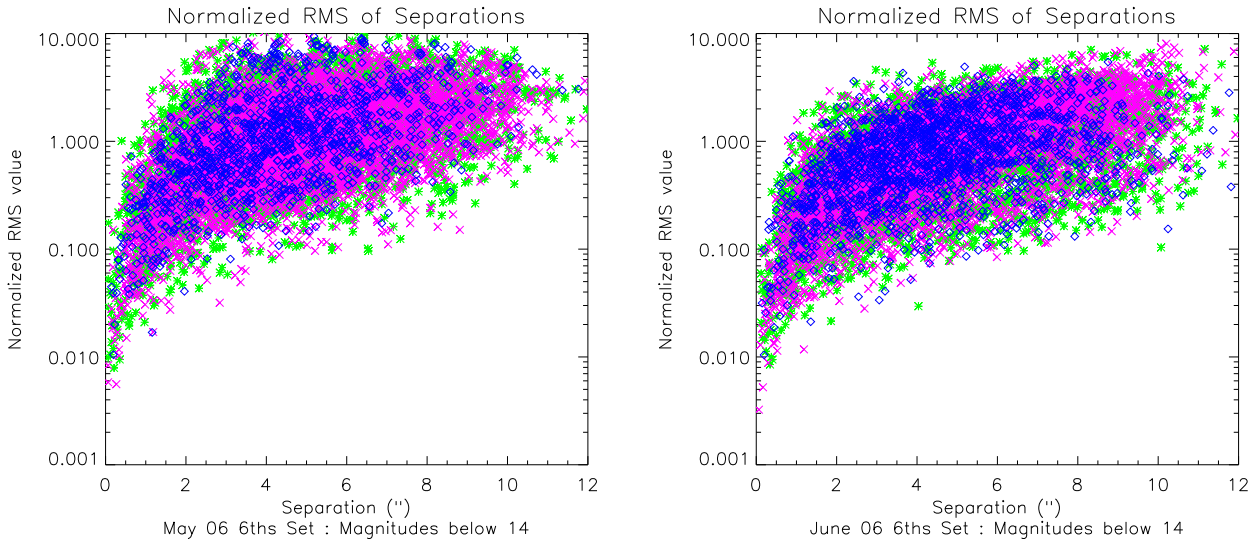

Fig. 4.— Plot of separation variance normalized by propogation error for $m_{K'} < 14$ stars versus Separation
Magenta indicates both stars had $m_{K'} > 12.5$
Green indicates one star had $m_{K'} \leq 12.5$ and one had $m_{K'} > 12.5$
Blue indicates both stars had $m_{K'} \leq 12.5$

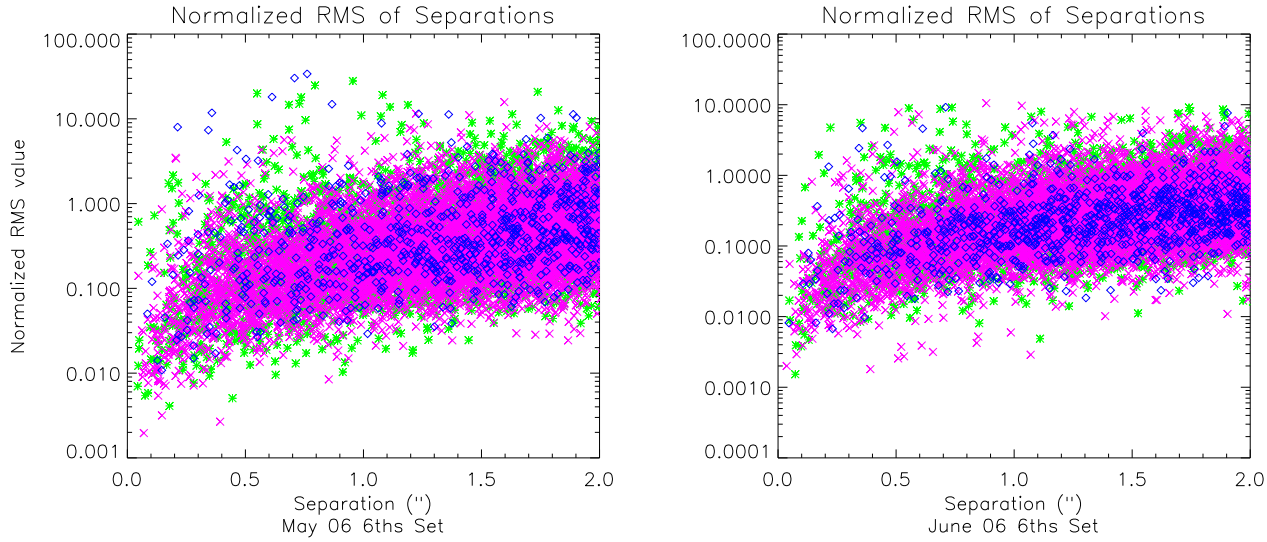

Fig. 5.— Plot of separation variance normalized by propogation error for $14 < m_{K'} < 16$ stars versus Separation
Magenta indicates both stars had $m_{K'} > 15$
Green indicates one star had $m_{K'} \leq 15$ and one had $m_{K'} > 15$
Blue indicates both stars had $m_{K'} \leq 15$

$T(\lambda)$ was taken to be a simple characteristic function centered on $\lambda_0 = 2.124$ with width: $\Delta\lambda = 0.35\ \mu m$ (Keck homepage).

$$\lambda_{eff} = \frac{\int T(\lambda)F(\lambda)\lambda d\lambda}{\int T(\lambda)F(\lambda)d\lambda} \rightarrow \frac{\int F(\lambda)\lambda d\lambda}{\int F(\lambda)d\lambda} \tag{3}$$

The stars' calibrated H and K magnitudes [S. A. Wright et al. 2006, in preparation], were converted to fluxes with the references ($F_H = 1050$ Jy and $F_K = 650$ Jy) to estimate the $F(\lambda)$, and then the λ_{eff}. An expression for the angular deviation of light was obtained by first applying Snell's law to an interface in the Earth's atmosphere: For a set wavelength, the difference in refractive index above and below is related to the difference in densities, where density is assumed to follow a simple Boltzmann relation, i.e.

$$\rho(h) = \rho_0 e^{-mgh/k_B T}. \tag{4}$$

Variation with height in temperature, T, and gravitational acceleration, g are neglected, and m is the mean mass of an air molecule. Hardy (1998) gives the dependence on wavelength in terms of the refractivity (defined as $10^6(n-1)$):

$$N_s(\lambda) = 10^6(8.34213 \times 10^{-5} + \frac{2.40603 \times 10^{-2}}{130 - \lambda^{-2}} + \frac{1.5997 \times 10^{-4}}{38.9 - \lambda^{-2}}) \tag{5}$$

(except that the cited reference has no 10^6, which this author assumes was a typographical error). The total deviation can then be computed numerically, adding each

$$\Delta\zeta = \frac{N_\lambda(e^{-mgh/k_B T} - e^{-mg(h-\Delta h)/k_B T})}{N_\lambda(e^{-mg(h-\Delta h)/k_B T}) + 10^6} \tan(\zeta) \tag{6}$$

from a height of one hundred kilometers down to the telescope's height of 4.2 kilometers, by 5 meter increments.

The zenith angle changes very slightly so a plot of stellar positions throughout the night should show a quasi-linear trend with airmass (where airmass is defined as: $\alpha = \sec(\zeta)$ so $\tan(\zeta) = \sqrt{\alpha^2 + 1}$). The plot (figure 6) displays the expected trend for pairings IR1-16C, and 16CC-16NE. The prominence of the former pair fits expectations based on average separation and the λ_{eff}, but it is curious that the latter pair stands out above others with lower average separations and larger λ_{eff}. Also, the actual scale of the effect is nearly a factor of ten larger than expected.

A common instrumental correction to dispersion in optical wavelengths is made with a Risley prism (Hardy 1998). An advantage of this device is keeping all of the light minus *s*light absorption. Some issues are the feasibility of applying this to Keck near-IR obseravtions, and another possible addition to optics errors. The angular differences become a hundredth as large using Keck's narrowband filter ($\Delta\lambda = 0.035\mu m$) but reducing the flux by a factor of ten adds 2.5 to every star's magnitude so this is counterproductive.

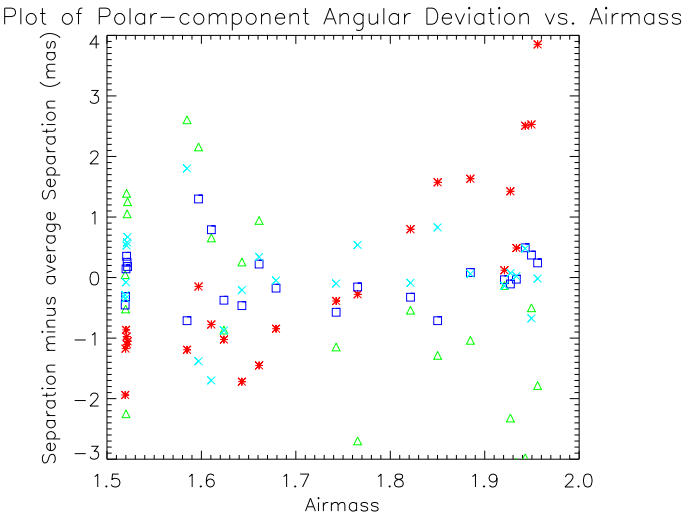

Fig. 6.— A plot of the deviation from the mean for the separations of stars IR1-16C (asterix), 16CC-16NE (triangles), 16C-16CC (squares), and 16C-16SW (x's). A linear trend is fairly evident with IR1-16C and 16CC-16NE separations, but not with the others.

5. Conclusion

Conditions at the $m_{K'} < 14$ level seem ripe for starting a baseline of measurements that would reveal the non-Keplerian features of orbits, but questionable where apparent K' magnitudes are between 14 and 16. This range describes the S0-cluster stars; the ones that provide the orbital data. Most of this error would appear to come from residual wavefront distortions, and analysis suggests that corrections for dispersion may also be required. Provided some satisfactory compensation for dispersion were found, however, great improvement might be achieved using a wider filter to increase the flux and decrease stellar magnitudes so the S0 stars at the 14-16 level drop to the desirable $m_{K'} < 14$.

The author thanks Professor Ghez, Seth Hornstein, Jessica Lu, Andrea Stolte, and the rest of the UCLA Galactic Center research group who were very generous with their time, assistance, and patience. Support for the author's undergraduate research exchange program was provided by the NSF. The data presented herein were obtained at the W.M. Keck Observatory, which is operated as a scientific partnership among the California Institute of Technology, the University of California and the National Aeronautics and Space Administration. The Observatory was made possible by the generous financial support of the W.M. Keck Foundation. The author wishes to recognize and acknowledge the very significant cultural role that the summit of Mauna Kea has always had within the indigenous Hawaiian community. We are most fortunate to have the opportunity to conduct observations from

this mountain

REFERENCES

Diolaiti, E., Bendinelli, O., Bonnacini, D., Close, L. M., Currie, D. G., & Parmeggiani, G., 2000, Proc. SPIE, 4007, 879

Ghez, A.M., Klein, B.L., Morris, M., Becklin, E.E., 1998, ApJ, 509, 678-686, High Proper-Motion Stars in the Vicinity of Saggittarius A*: Evidence for a Supermassive Black Hole at the Center of our Galaxy

Ghez, A.M., Morris, M., Tanner, A., Kremenek T., 2000, Letters to Nature, 407, 349-51, The Accelerations of Stars Orbiting the Milky Way's Central Black Hole

Ghez, A. M., Salim, S., Hornstein, S. D., Tanner, A., Morris, M., Becklin, E. E., Duchene, G., 2005, ApJ, 620, 744, Stellar Oribts Around the Galactic Center Black Hole

Ghez et al., 2003, ApJ, 586, L127-L131, The First Measurement of Spectral Lines in a Short-Period Star Bound to the Galaxy's Central Black Hole: a Paradox of Youth

Hardy, J. W.,Adaptive Optics for Astronomical Telescopes Oxford 1998

Jiang, H. X., & Lin, J. Y., 1985, Am. J. Phys., 53, 694

Keck homepage 28 August 2006, http://www.keckobservatory.org

Pyraf homepage: 28 August 2006, http://www.stsci.edu/resources/software_hardware/pyraf

Rubilar, G.F. & Eckart, A., 2001, A&A, 374:95-104, Periastron Shifts of Stellar Orbits near the Galactic Center

Table 1. Fits of the form, $\sigma_{frames} = \sigma_{floor} + A/\sqrt{N}$, for several magnitude bins

2006;	$13 < m_{K'} \leq 14$	$14 < m_{K'} \leq 15$	$15 < m_{K'} \leq 16$
May	.16±.07+(1.1±.25)/$\sqrt{N}$	.24±.07+(1.1±.26)/$\sqrt{N}$	.40±.10+(1.1±.39)/$\sqrt{N}$
June	.19±.06 + (.79±.22)/$\sqrt{N}$	.25±.05+(.95±.20)/$\sqrt{N}$	.39±.08+(1.0±.30)$\sqrt{N}$

Table 2. Stars for dispersion analysis with their H and K magnitudes, and estimated effective wavelengths

Star Name	m_H[a]	m_K[a]	λ_{eff} (μm)
IR-1	14.89	14.21	2.1265
16C	11.94	9.792	2.1396
16CC	12.47	10.56	2.1384
16NE	12.08	10.06	2.1386
16SW	11.65	10.02	2.1365

[a]Apparent magnitudes where H is $\lambda = 1.65\mu m$, and K is $\lambda = 2.20\mu m$

Table 3. Expected angular differences due to dispersion

Star pairing	$\bar{S}$ in arsec.[a]	S_p for $\zeta_0 = 48^{o}$[b]	S_p for $\zeta_0 = 60^{o}$[b]
IR1-16C	1.698	0.566	0.883
16CC-16NE	0.984	0.011	0.016
16C-16CC	0.911	0.052	0.082
16C-16SW	1.483	0.131	0.205

[a]Average separation

[b]Predicted change in separation (North-axis) due to disperion.